Fluid Simulations and Theory of Boundary Plasma Fluctuations [1]

R.H. Cohen[1)], B. LaBombard[2)], L.L. LoDestro[1)], T.D. Rognlienr[1)], D.D. Ryutov[1)], J.L. Terry[1)], M.V. Umansky[1)], X.Q. Xu[1)], S. Zweben[3)]

[1)] Lawrence Livermore National Laboratory, Livermore CA 94550 USA
[2)] Massachusetts Institute of Technology, Cambridge, MA 02139 USA
[3)] Princeton Plasma Physics Laboratory, Princeon, NJ 08540 USA

e-mail contact of main author: rcohen@llnl.gov

Abstract. Computational and theoretical investigations are presented of boundary-plasma microturbulence that take into accont important effects of the geometry of diverted tokamaks. These include BOUT studies of Alcator C-Mod and preliminary comparisons with experimental data; self-consistent calculation of edge turbulence and transport via coupling of BOUT with the UEDGE edge transport code; analytic theory and simulation evidence for instabilities confined to divertor legs, and analytic studies of "blobs" in the main-scrape-off-laye and divertor-leg regions in the presence of x-point magnetic shear.

1. Introduction

Turbulent transport in the boundary plasma of tokamaks play an essential role in establishing the boundary conditions for core-plasma transport and in establishing the pattern of power and particle loss to bounding material surfaces. We present here recent computational and analytic studies of such phenomena which take into account important effects of the magnetic geometry. These include: the first studies with the BOUT two-fluid turbulence code that take into account the effects of the asymmetric double-null divertor geometry (Sec. 2), along with experimental comparisons for the C-Mod tokamak; self-consistent calculation of edge turbulence and transport via relaxed iterative coupling (RIC) [1] (Sec. 3), an analysis of instabilities confined to divertor legs (Sec. 4), and a discussion of geometrical effects on propagation of "blobs" (large intermittent propagating structures, elongated along magnetic-field lines) (Sec. 5). A discussion is presented in Sec. 6.

2. BOUT Simulations

We have conducted simulation of edge turubulence for the MIT Alcator C-Mod tokamak with the BOUT code [2]. Edge plasma in C-Mod is relatively dense ($n_i \sim 0.5 \times 10^{20}$ m^{-3}) and cold ($T_e \sim 30$ eV) that makes C-Mod a particularly good choice for application of the Braginski-based plasma model. For the present simulation a particular C-Mod shot 1031204007, t=740 mS was used to set up the magnetic geometry based on EFIT reconstruction and the profiles of background plasma density and temperature based on data from the scanning Langmuir probe.

Two simulation cases were considered, in one treating the magnetic equilibrium as a lower single null (LSN), and in the other extending the domain to include the secondary x-point as in full unbalanced double-null (UDN).

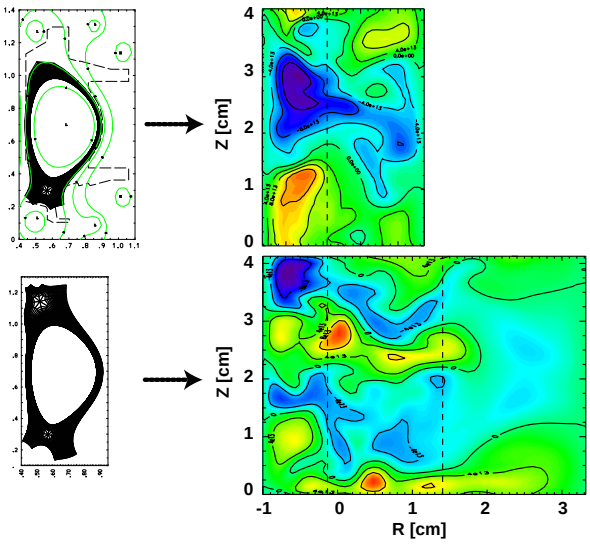

FIG. 1: Fluctuations of density at outer midplane for single-null and double-null BOUT runs

[1]Work performed for the U.S. Department of Energy under contracts W7405-ENG-48 at U.C. LLNL and DE-AC02-76CHO3073 at PPPL, and Cooperatove Agreement DE-FC02-99-ER54512 at MIT

The considered configuration is nominally LSN and the first simulation case was done in LSN geometry. As usual, the simulation was done by starting from a small instabilty seed and allowing the system to evolve through linear instability and on into saturated turbulence. The evolution of turbulent plasma was followed for $\sim$ 500 ms, spanning many dozens of eddy turn-around times. The appearance of turbulent eddies was qualititively similar to that typically observed in the experiment with the fast cameras.

To make a quantitative comparison with the experiment a statistical analysis was performed and basic parameters such as the auto-correlation time, τ, and auto-correlation lengths in the radial, L_{rad}, and poloidal,L_{pol}, directions were determined. The value of L_{pol} was found to be in the range of typical experimental values, $\sim$ 0.5-1.0 cm, while L_{rad} was smaller than experimental values $\sim$ 0.5-1.5 cm. However the radial domain size for the LSN case was just $\sim$ 2 cm, constrained by the location of the secondary separatrix, and it was conjectured that the outer boundary condition (zero fluctuation amplitude) was affecting the solution.

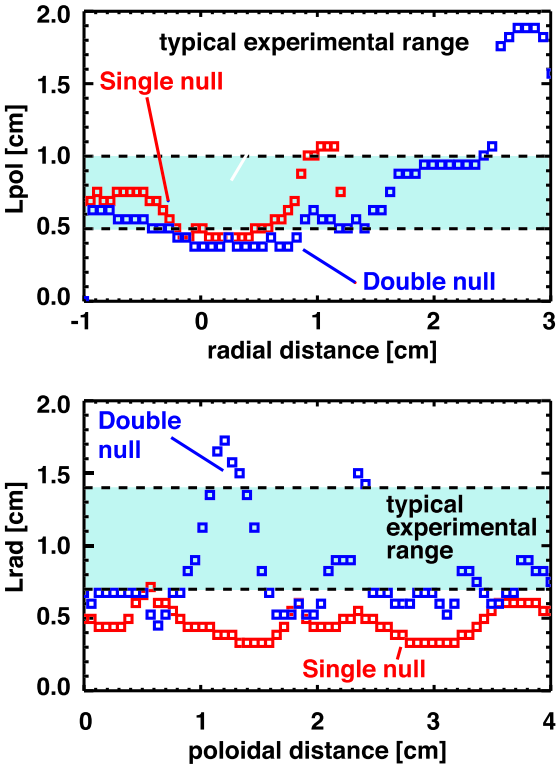

FIG. 2: Correlation lengths for fluctuating density at outer midplane for single-null and double-null BOUT runs

That motivated re-running same case as a UDN which allowed to substantially extend the radial domain further out. Comparison of the two cases is done in Fig. 1 where one can see that in the UDN case turbulent structures are more extended radially compared to the LSN case. That is confirmed by Fig. 2 where L_{rad} and L_{pol} are plotted vs. the poloidal and radial coordinates repectively. The experimental correlations lengths were not radially resolved; the shaded area denotes the averages over all radii. One can see in Fig. 2 that L_{pol} is quite similar for the two cases, as expected, while L_{rad} is considerably large for the UDN case.

The remaining issue still investigated is matching of the auto-correlation times where the agreement is not as good. The auto-correlation times (defined as the time for the autocorrelation function to fall to 0.5) inferred from both cases was about 2 μs, considerably smaller than the experimentally known value (by a factor of around 5).

3. Transport-Turbulence Coupling

The self-consistent model of the long-term evolution of the edge plasma profile requires coupling the turbulence simulation with a transport simulation. Because the timescale of turbulence growth and saturation is typically a few of orders of magnitude smaller than the edge profile evolution time to steady state, we have continued to investigate the computational efficiency of coupling the turbulence and transport simulations on their own timescales by coupling 3D BOUT [2] for turbulence and 2D (axisymetric) UEDGE [3] for transport. We have extended the initial coupling work reported at the FEC 2004 meeting [4] to include multiple plasma variables [5] and also have examined the impact of intermittency.

The coupling scheme utilizes the general Relaxed Iterative Coupling (RIC) method developed

in Ref. [1]. This technique is illustrated by the continuity equation for the ion density n_i is separated into two equations, one describing the long-time evolution of the temporally- and toroidally-averaged density, $N_i \equiv \langle n_i \rangle_{\phi,t}$, and the second giving the rapidly varying fluctuations $\tilde{n_i} \equiv n_i - N_i$, yielding

$$\partial_t N_i + \nabla \cdot \langle \Gamma \rangle = \langle S \rangle \quad \text{and} \quad \partial_t \tilde{n_i} + \nabla \cdot (\Gamma - \langle \Gamma \rangle) = S - \langle S \rangle. \tag{1}$$

The radial particle flux, Γ_r, is generally dominated by a large turbulence-enduced component provide by the BOUT. The RIC scheme can be used to provide time-dependent evolution, but here we focus on steady-state solutions. To maintain numerical stability [1], the turbulent fluxes from BOUT and the profiles from UEDGE are obtained through a series of iterative steps designated by the index m, such that for the m^{th} iteration the flux is $\langle \Gamma_r \rangle^m = (1-\alpha_1)\langle \tilde{n_i} \tilde{v_r} \rangle^{m-1} + \alpha_1 \langle \tilde{n_i} \tilde{v_r} \rangle^m$, where α_1 is a relaxation factor. The UEDGE profile information used by BOUT is likewise fractional combination of previous and present profiles associated with the m^{th} iteration with relaxation parameter α_2.

For multiple variable coupling to model DIII-D single-null edge plasmas, we found that it was necessary to separate the representation of the turbulent flux in UEDGE by a combination of diffusion and convection because fluxes in some regions were in the direction of up the local gradient, implying a negative (and thus numerically unstable) diffusion coefficient. The mix of diffusion and convection in the transport code is not important as long as negative diffusion is avoided and the total turbulent flux is faithfully represented. An example of such coupling was considered for the magnetic equilibrium from DIII-D discharge 107404 with the core-boundary density of 2.5×10^{19} m^{-3} and core-boundary temperatures of $T_e = T_i = 200$ eV [5]. Here no radial electric field is present, so the model corresponds to the L-mode phase. The turbulent fluxes of ion density and separate electron and ion temperatures, n_i, T_e, T_i, from BOUT are fit by separate diffusive and convection coefficients such that 50% of the flux is carried by each. A plot of the effective convective velocities for each of the three variables is show in Fig. 3 after 7 iterations with the rather aggressive $\alpha_{1,2} = 0.5$, and the profiles and fluxes appeared to be approaching an approximate quasi-steady state. Beyond $m = 7$, the sudden growth of a large T_e fluctuation near the wall boundary of that exceeded a physics limit in BOUT (possibly related to boundary conditions), interrupting further iterations. Longer iterative sequences are discussed in the following

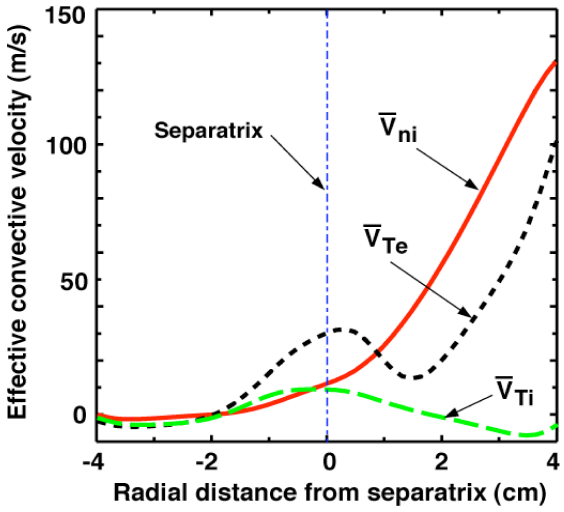

FIG. 3: The effective convective velocities for n_i, T_e, and T_i for a BOUT/UEDGE coupling of a DIII-D single-null geometry [5].

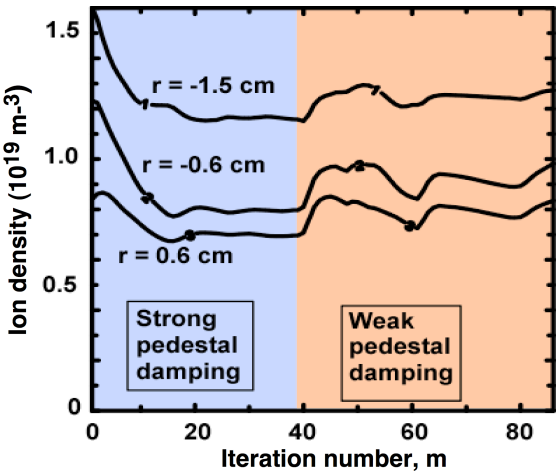

FIG. 4: Ion density at three radial locations versus iteration number, m, for a limiter simulation of a toroidal annulus with a 6 cm radial width where $r = 0$ corresponds to the separatrix determine by an outboard limiter insert to this location. The range $m < 40$ corresponds to case 1, and $m \geq 40$ corresponds to case 2.

paragraph. The convective velocities shown in Fig. 3 are of the same shape and magnitude as that reported from experimental observations in DIII-D and Alcator C-Mod [6].

To further investigate the coupling for a longer iteration sequence and to assess the role of intermittency, we perform a series of simulations for a circular tokamak geometry with an outboard midplane limiter inserted half-way into the radial domain, which has a total width of 6 cm. Here the core-boundary density and temperatures are set to $n_i = 2.5 \times 10^{19}$ m^{-3} and $T_{e,i} = 100$ eV. Instability mechanisms present include for both curvature- and sheath-driven modes. Three different cases are examined to produce a range of turbulence characteristics, especially strongly intermittent versus moderately intermittent. Case 1 adds a damping term in the vicinity of each radial boundary but that decays to 1/e at 1.5 cm from the boundary. This damping acts to suppress turbulence in the inner half of the closed-field-line region. Turbulence appears to be driven in the radial location of the limiter while spreading part-way into the closed- and open-field-line regions. Here a moderate level of intermittency results after an initial transience, and a long-time quasi-steady state is reached for the BOUT/UEDGE coupling using $\alpha_{1,2} = 0.25$ as shown by the density at several radial location in Fig. 4 up to $m = 39$. As as above, the turbulent fluxes in UEDGE are prescribed to be represented half each by diffusion and convection. The corresponding effective density diffusion coefficient , D_{eff}, is shown in Fig. 5.

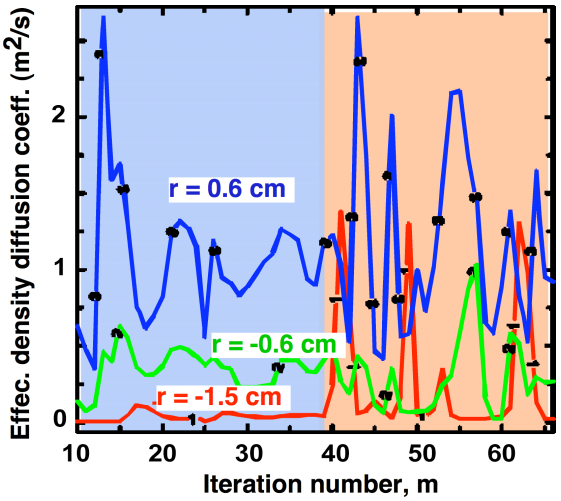

FIG. 5: Effective density diffusion versus iteration number for cases 1 and 2 shown in Fig. 4.

Two other variations of this case are considered: Case 2 reduces the decay scale-length of the boundary damping by 1/2, and then the turbulence has the added component of a large, but more intermittent mode in the closed field-line region, presumably associated with the curvature drive. The results for density and D_{eff} are shown in Figs. 4-5 for $m = 40 - 83$. Note that while the coupling does not diverge, the density does not reach a quasi-steady state, but rather has periodic increases in response to the larger transport events, especially in the closed field-line region, even though $\alpha_{1,2} = 0.25$. Clearly, these density perturbations would become even more prominent for less-relaxed coupling, likely impacting the instability drive more strongly as well. The third case is like case 2, except that a radial electric field well is imposed in the core region in an approximately parabolic form with a minimum midway between the inner boundary and the limiter and a net depth of ~ 20 kV/m. This E_r model is used to approximate what might be expected in the more quiescent H-mode operation. For this case, the E_r largely suppresses the strong mode in the closed-field-line region, and the spectrum reverts to a value close to that for case 1, except that know there is substantial poloidal shear-flow induced by the radial field well. Likewise, the density at various locations appear to again reach a well-defined quasi-steady state (not shown here).

The RIC coupling of edge transport and turbulence can be efficient for cases with weak-to-moderate intermittency owing to the large timescale separation. For sufficiently strong and intermittent turbulence, the relaxation method clearly misses rapid features of the dynamic response to the large events. For the latter case, the extent to which the relaxation method distorts profile evolution needs to be evaluated by direct comparison of coupling that follows the time-dependence of the profile evolution during the large transport event, which can also be done by having BOUT evolve its own profiles. For periods of low to moderate turbulence, such as between ELMs, the RIC coupling presented appears promising when utilized in a time-dependent

mode.

4. Divertor-Leg and Private-Flux Instabilities

The plasma in the divertor is in direct contact with the divertor plates and, therefore, may be strongly affected by the sheath boundary conditions. In the private flux region there is obviously no connection with the main SOL along magnetic-field lines. In the common flux region the connection is present but may be strongly reduced by the shear near the X-point. As noted in Refs. [7, 8, 9] these features can be used to reduce the divertor heat load by exploiting various instabilities specific to the divertor plasma so that the plasma cross-field diffusion in the divertor legs would be maximized and lead to a broadening of the wetted area. On the other hand, the possibility of confining these instabilities within divertor, without inducing additional transport in the main SOL, would eliminate any adverse effect of these instabilities on the pedestal formation and bulk plasma confinement. This approach generally favors divertors with long legs and can therefore improve performance of the X divertor [10].

In this paper we present an analysis of divertor-leg instabilities that consistently includes curvature, x-point shear and sheath boundary conditions; we discuss the consequences for instabilities in the private flux region. We use the generic divertor geometry shown in Fig. 6. The angle α is considered positive when the tilt of the divertor plate is as shown in Fig. 6. We assume that the distance ℓ_D from the X-point to the divertor plate is ~ 20 cm, $B_T \sim 5$ T, $B_P \sim 0.3$ T at the divertor floor, $T_e \sim 25$ eV, and its cross-field length-scale $\Delta \sim 1$ cm in the private-flux region at the divertor plate, and$n \sim 10^{13}$ cm^{-3}. These parameters roughly correspond to those of a high-field compact tokamak like C-Mod, although they do not reflect details of any particular tokamak. We assume also that the plasma fills the whole flux-tube connecting the inner end outer strike points, neglecting variation of the parameters along the flux tube.

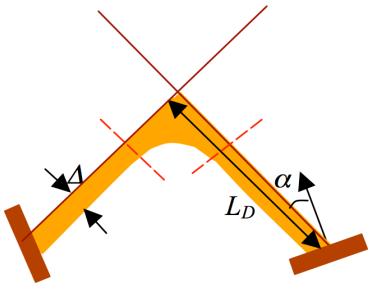

FIG. 6: Schematic of the private flux region Dashed lines represent the "control planes". The major axis is to the left.

We consider unstable modes satisfying $\Delta^{-1} < k_\perp < \rho_i^{-1}$, where $\rho_i = c_s/omegaci$ with $c_s = (2T_e/m)^{1/2}$. As the private flux plasma has very low beta, electrostatics is sufficient. (We can verify a posteriori that resistive ballooning is insignificant). The modes are flute-like, with $k_\parallel \ll k_\perp$. For the set of parameters mentioned above, $\rho_i \sim 0.02$ cm (deuterium). An important factor is the squeezing of the flux tubes on their way from one strike point to the other, caused by strong shear near the X point [11, 12]. A flux tube that is circular at one of strike point and centered a distance Δ_0 from the separatrix ends up having a highly stretched elliptical cross-section, with ellipticity $E \approx \ell_D/\Delta_0$. Hence a perturbation with wavenumber $k_\perp$ at the outer strike point has a scale length $(k_\perp E)^{-1} \sim k_\perp^{-1}\Delta_0/\ell_D$ near the inner strike-point. If this scale-length becomes less than ρ_i, the perturbation is dissolved in the ambient plasma. In this case perturbations in the two legs are disconnected and the effect of the x-point shear can be approximated by the "heuristic boundary condition" [2] on control planes situated somewhat below the X-point (dashed lines in Fig. 6). Conversely, if $k_\perp\Delta_0/\ell_D > \rho_i$ the perturbation connects the two strike points. Estimating $\Delta_0 \approx \Delta/2$, one finds that the disconnection occurs for the perturbations with $k_\perp\rho_i > \Delta/2L_D \sim 1/40$, *i.e.*, even for perturbations with the cross-field length-scale approaching the plasma thickness Δ. Therefore, we consider only disconnected perturbations.

We include in the analysis the following factors: a sheath boundary condition at the divertor plate, with the effects of tilt ($\sin\alpha \neq 0$) and plasma drifts included; the heuristic boundary condition at the control surface; and magnetic field curvature. We assume $T_e^{-1}\nabla_\perp T_e \gg n^{-1}\nabla_\perp n$ and

neglect the latter. In the eikonal approximation, we arrive at the following dispersion relation:

$$\Omega^2 + \Omega(i\Omega_1 + \Omega_2 + i\Omega_3) - i\Gamma_1^2 - \Gamma_2^2 - \Gamma_3^2 = 0 \tag{2}$$

with

$$\Omega_1 = \frac{\omega_{ci}^2 m_i c_s}{L_\parallel k_\perp^2 T_e}, \quad \Omega_2 = \frac{\omega_{ci}}{k_\perp L_\parallel}\frac{B}{B_p}\tan\alpha, \quad \Omega_3 = \frac{\omega_{ci} G}{k_\perp L_\parallel}, \tag{3}$$

$$\Gamma_1^2 = \frac{\hat{\Lambda}\omega_{ci} c_s}{k_\perp L_\parallel \Delta}, \quad \Gamma_2^2 = \pm\frac{T_e}{m_i L_\parallel \Delta}\tan\alpha, \quad \Gamma_3^2 = \pm T_e m_i R\Delta \tag{4}$$

with $L_\parallel$ the distance along a field line from the divertor plate to the control surface, and the constant $\hat{\Lambda} \sim (1/2)\ln m_e/m_i \sim 4$. Here G is an adjustment factor of order one that enters the heuristic boundary condition **??**, and R is evaluated at the strike point. The "plus" ("minus") sign corresponds to the outer (inner) leg.

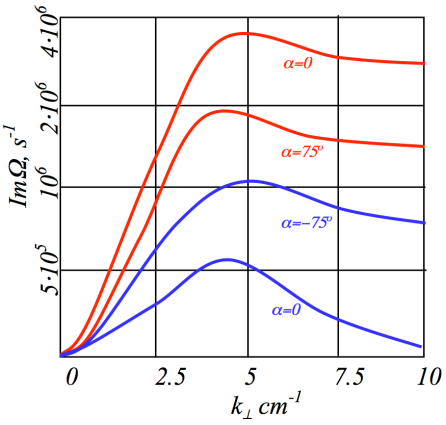

FIG. 7: Growth rate versus wavenumber. Red (blue) cuves correspond to the inner(outer) leg. Note significant increase in growth rate in the outer leg for negative tilt.

The first term in the left hand side (LHS) of Eq. (1) describes plasma inertia. The last term describes curvature stabilization (destabilization) of perturbations: in the private flux region, for the outer leg, it is stabilizing, whereas for the inner leg it is de-stabilizing. The second to the last term describes the stabilizing/destabilizing effect the divertor-plate tilt. In order to have stronger turbulent broadening of the private flux region it is desirable to have $\alpha < 0 (> 0)$ in the outer (inner) leg. The Ω_3 term describes the effect of the x-point-shear boundary condition. The rest of the terms come from the sheath boundary condition (Cf. [8]). Figure 7 shows the dependence of the growth rate vs. wave number. For $R \sim 0.5$ m and $L_\parallel \sim 3$ m, one sees that the tilt term dominates over the curvature term for a strong-enough tilt, $90° - \alpha < 15°$. Near the maxima, the real part of the frequency is of the order of the growth rate, i.e., $f = \mathrm{Re}\Omega/2\pi \sim \mathrm{Im}\Omega/2\pi \sim 100$ kHz. The diffusion coefficient evaluated by a mixing length estimate is quite high, approaching 5 m^2/s (i.e., significantly higher than Bohm). At the non-linear stage of the instability, one can expect formation of blobs [13] moving away from the separatrix, deeper into the private flux region. This is discussed in the next section.

5. Blobs

A number of experiments (*e.g.*,, Refs. [14, 15, 16]) have observed large-amplitude, intermittant, strongly elongated (along the magnetic field) structures, or "blobs". They are of considerable importance, since they propagate radially and can be a significant transport mechanism to the main chamber walls. A simple model was proposed in Ref. [17]; more recent treatments have introduced the breaking effect of contact with external walls [18, 19], and more quantitative analyses based on the vorticity equation [19, 20].

In the past few years it has been recognized that blobs (like lower-amplitude fluctations in the edge) can be strongly impacted by the presence of x-point shear, and the effects can be analyzed using the "heuristic boundary condition" described in Sec. 4. Ref. [18] derived the terminal velocity of a blob in contact with the x-point region. Recently we pointed out [9, 21] a number of further consequences of x points and wall contact (or lack thereof) for blob dynamics. Here we collect these results, comment on some aspects that were not explicitly treated previously,

and then consider the implications for blob propagation in C-Mod, where some rather detailed studies of blob propagation have been performed.

The salient results from Refs. [9, 21] are: (1) The x points decouple blobs and blob dynamics in the main SOL and in the divertor legs. Blobs born close to the separatrix in either the main SOL or the divertor leg will be confined to that region until they have propagated out far enough that the x-point shearing is sufficiently weak. The terminal velocity of a blob so constrained is of order $\dot{R}_x = v_{ti}L_x\rho/GRa$ where L_x is the field line connection length (half the field line length) to the x point region, a is the blob radius, ρ is the gyrordius, and G is the order-unity phenomenological constant in the x-point heuristic boundary condition. (2) Divertor leg instabilities, such as are discussed in Sec. 4., can grow into blobs localized to the divertor legs. (3) Blobs which may from birth extend all the way from the main SOL to the divertor floor, will in effect move independently in the man SOL and diveror. (4) when a blob has propagated sufficiently far from the separatrix that x-point shear is insufficient to bring the blob thickness down to the gyroradius, it ceases to be confined poloidally to one side or the other of the x-point region. (We estimate in the next paragraph where this occurs). The blob then enters a period of acceleration (characteristic of an completely isolated blob, with acceleration rate $\ddot{R}_i \sim v_{ti}^2/R$), while simutaneously expanding along the magnetic field at thermal speed, until the blob reaches some other bounding surface. (5) For a blob in contact with a material surface, and for which the pressure or density distribution within the blob cross section is non-symmetric, experiences a conducting-wall drive in addition to the better-known curvature drive. These blobs are the nonlinear limit of the conducting-wall temperature-gradient modes described in Ref. [22]. The terminal velocity in the case where this drive dominates over curvature drive (valid for $\Lambda aRF_a/\rho_i L_c > 1$, where $\Lambda \sim 4$ and $F_a < 1$ is a measure of the degree of asymmetry of the pressure and density distributions) is $\dot{R}_{cw} \sim F_a\Lambda\rho_s c_s/a$; in the opposite limit, it is $\dot{R}_\kappa \sim (\rho_s^2 c_s L_c/Ra^2)(1 + T_i/T_e)$.

The question of how far from the separatrix the x point is effective in isolating a blob has not been explicitly dealt with in the previous literature. An estimate for the critical distance from the separatrix Δ_c proceeds as follows: as noted in Ref. [23], a flux tube that is initially circular far above the x point, with radius a and distance from the separatrix Δ, is elliptically distorted to have a thickness $\delta R \approx a\Delta/(\ell_d + (r_d\Delta)^{1/2})$ at a poloidal distance ℓ_d below the x point (up to the limit where the quadrupolar approximate for the poloidal field breaks down, *i.e.* up to $\ell_d \sim r_d$, where $r_d \sim$ minor radius is the poloidal distance over which the poloidal field projected from the quadrupolar approximation is equal to the main-SOL poloidal field). Since the flux tube continues to shrink up to the limit of applicability of the ellipticity expression, it is tempting to evaluate the criterion for Δ_c by solving for $\delta R = \rho$ at the divertor plate (or at the limiting value $\ell_d = r_d$). However, we argue that the correct limit is closer to the separatrix: as a flux tube propagates outward, the position along which the flux tube is squeezed to a specified thickness (in particular, a gyroradius) moves further away from the reference position (where the flux tube is circular). Once this position is beyond the x point by a distance of order $(r_d\Delta)^{1/2}$, this position advances faster than an expanding flux tube can keep up with it. This is easily verified: in the relevant limit, $\ell_d \sim a\Delta/\delta R$, so setting $\delta R = \rho$ and taking the time derivative we find $d\ell_d/dt \sim a\dot{R}/\rho$. Substituting in the expression $\dot{R}_x$ for $\dot{R}$, we find that $d\ell_d/dt \sim v_{ti}L_c/GR \gtrsim v_{ti}$, whereas thermal expansion of the blob projected onto the poloidal plane is only at the rate $v_{ti}B_p/B$. From this consideration we conclude that the limit of applicability of the heuristic boundary condition is at the field line where the blob thickness is shrunk to the ion gyroradius in the x-point region (ℓ_d *sim*0 in the expression for δR.) Evaluating this criterion we conclude that $\Delta_c \sim r_d(\rho/a)^2$. Blobs originating on one side or the other of the x point (either in the main SOL or the private flux region) at larger radii simply cannot expand fast enough along field lines to reach the location where they are squeezed to a gyroradius. We then note that for

blobs thicker than $(r_d\rho)^{1/2}$, the critical radius is itself as small as a gyroradius and the x-point limitation never comes into play.

Another useful criterion that can be extracted from Ref. [21] is the criterion that resistive ballooning isolate a blob from material endwalls. Eqs. (42) and (43) of Ref. [21] are equations for the evollution of the normal and geodesic component of displacement for a blob derived in the approximation of resistive MHD. The resistive ballooning limit prevails when the parallel derivative terms in those equations are negligible, from which we obtain the following criterion:

$$\dot{R} \ll \dot{R}_b = \beta c^2 L_c^2/\pi a^2 \sigma R \tag{5}$$

where σ is the parallel conductivity.

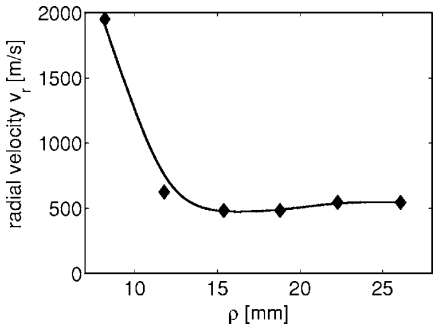

FIG. 8: Blob propagation speed in C-Mod, from Ref. [15].

We now consider application of these considerations to C-Mod. Ref. [15] contains a plot of blob velocity versus radius for a representative discharge, reproduced here as Fig. 8. A striking feature of that figure is that, apart from the large velocity shown at the smallest radius (which the authors regard as an instrumental artifact), the velocity is nearly constant, and in any case does not show much structure. One is then led to ask how to reconcile this with theoretical considerations that would have the blob motion accelerating or having various velocities depending on what surfaces the blob contacts and whether it passes close to the x point. This point is underscored by evaluation of the applicability condition for ballooning, Eq. (5). Blobs in C-mod are observed to have radii of order 1 cm (see e.g. Fig. 9 of ref. [15]). Hence for C-Mod nominal parameters, the ballooning criterion becomes $\dot{R} \ll \dot{R}_b \sim 110$ m/s$\times(n/10^{14}cm^{-3})(L_c/6\mathrm{m})^2(1\,\mathrm{cm}/a)^2(T/20\text{ ev})^{-1/2}$, which, for the observed blob velocity from Fig. 8 and typical C-mod parameters, is not satisfied except possibly very close to the separatrix where the field lines become very long. So indeed we must consider where blobs end. Because C-Mod is an especially high-field device (~ 5 T), the typical blob radius is marginally big enough to satisfy the criterion that x-poinit limitations never come into play; for somewhat smaller blobs, the x-point boundary condition is effective only for field lines within about a gyoradius (~ 0.2 mm) of the separatrix. The first data point in Fig. 8 is already at a radius that intersects the divertor throat; hence blobs are expected to move at a velocity limited by contact with conducting surfaces. Because, in particular, for $F_a \sim 1$, the criterion for dominance of conducting-wall drive is strongly satisfied, we obtain the estimate $\dot{R} = \dot{R}_{cw} \sim 730$ m/s $\times(T/20$ eV) (1 cm/$a)F_a$. This is of the right order of magnitude and could plausibly be consistent with a constant blob velocity if the asymmetry parameter F_a compensates for a decrease in blob temperature as it propagates. (Coincidentally, the propagation speed obtained from the x-point shear boundary condition near the separatrix is approximately the same – though we contend that this condition never applies for NSTX because of the small gyroradius relative to blob size.)

We return to the discussion of divertor-leg blobs, noted in the preceding section. If the electron temperature in the blob is uniform, the drive is associated with the curvature and the tilt of the divertor plates. The contact with the conducting divertor plate partially reduces the polarization field and gives rise to a constant-velocity motion. The x-point "heuristic boundary condition" turns out to be high resistance compared to the sheath, and so is effectively insulating. This leads to the estimate for the blob velocity, $\dot{R}_{dl} = (\rho_i^2 c_s/a^2)[(L_\parallel/R) \pm \tan\alpha$, where + (-) corresponds to the inner(outer) divertor leg in the private flux region, and opposite for the common flux. If the tilt term dominates over the curvature term by O(1), blob motion is strong enough to strongly affect transport; the ion parallel transit time is longer than the blob propagation time over the

SOL width Δ even for blobs with size Δ for the parameters of Sec. 4. If the broadening is sufficient to result in reconnection of the inner and outer strike points in the private flux region, and there is enough tilt with favorable signs at both plates, further broadening is possible.

6. Conclusion

From the studies presented here, we can draw the following conclusions: (1) BOUT fluid simulations are increasingly in agreement with measurements of fluctuations in C-Mod; (2) self-consistent computation edge turbulence and transport via the RIC method has been demonstrated for multi-variable coupling, for the case of relatively steady turbulence, but challenges remain for the case of strong intermittant transport; (3) Curvature- and sheath-driven instabilities can exist in the private- as well as common-flux regions of divertor legs, isolated from the main SOL; these offer the possibility of broadening the SOL without impacting the main plasma. vertor-plate tilt can significantly increase the growth rate. Nonlinearly these can develop into divertor-leg blobs; (4) X-point effects can isolate blobs in the main SOL from divertor legs, and non-symmetric blobs in contact with material sufaces can be dominated by sheath-impedance drive. This is consistent with the magnitude and relative constancy of C-Mod blob velocities reported in Ref. [15]. The X-point effects likely have little role in those reported measurements.

References

[1] SHESTAKOV, A.I., COHEN, R.H., CROTINGER, J.A., LODESTRO, L.L., TARDITI, A., XU, X.Q., J. Comp. Phys. **185** (2003) 399; corrigendum: J. Comp. Phys. **186** (2003) 360.
[2] XU, X.Q., COHEN, R.H., ROGNLIEN, T.D., MYRA, J.R., Phys. Plasmas **7** (2000) 1951.
[3] ROGNLIEN, T.D., RYUTOV, D.D., MATTOR, N., PORTER, G.D., Phys. Plasmas **6** (1999) 1851.
[4] XU, X.Q. et al., 20th IAEA Fusion Energy Conf., Villamoura, paper IAEA-CSP-25/TH1-5 (IAEA, Vienna, 2005).
[5] ROGNLIEN, T.D., UMANSKY, M.V., XU, X.Q., COHEN, R.H., LODESTRO, L.L., J. Nucl. Mater. **337-339** (2005) 327.
[6] LIPSCHULTZ, B., WHYTE, D., LABOMBARD, B., Plasma Phys. Contr. Fusion **47** (2005) 1559.
[7] COHEN, R.H., RYUTOV, D.D., Nucl. Fusion bf 37 (1997) 621
[8] RYUTOV, D.D. Contrib. Plasma Phys. **44** (2004) 168.
[9] COHEN, R.H., RYUTOV, D.D. Contrib. Plasma Phys. **46** (2006) 678.
[10] KOTSCHENREUTHER, M., private communication (2006).
[11] FARINA, D., POZZOLI, R., RYUTOV, D.D., Nucl. Fuson **33** (1993) 1315.
[12] COHEN, R.H., RYUTOV, D.D. Contrib. Plasma Phys. **36** (1996) 161.
[13] KRASHENINNIKOV, S, Phys. Lett. **A 283**, 368 (2001).
[14] TERRY, J.L., ZWEBEN, S.J., HALLATSCHEK, K., LABOBMARD, B., MAQUEDA, R.J., BAI, B., BOSWELL, C.J., GREENWALD, M., KOPON, D., NEVINS, W.M., PITCHER, C.S., ROGERS, B.N., STOTLER, D.P., XU, X.Q., Phys. Plasmas **10** (2003) 1739.
[15] GRULKE, G., TERRY, J.L., LABOBMBARD, B., ZWEBEN, S.J., Phys. Plasmas **13** (2006) 012306.
[16] ZWEBEN, S.J., MACQUEDDA, R.J., TERRY, J.L., MUNSAT, T., MYRA, J.R., D'IPPOLITO, D., RUSSELL, D.A., KROMMES, J.A., LEBLANC, B., STOLZFUS-DUECK, T., STOTLER, D.P., WILLIAMS, K.M., BUSH, C.E., MAINGI, R., GRULKE, O., SABBAGH, S.A., WHITE, A.E., Phys. Plasmas **13** (2006) 056114.
[17] KRASHENINNIKOV, S.I.,, Phys. Lett. **A 283** (2001) 368.

[18] KRASHENINNIKOV, S.I., RYUTOV, D.D., YU, G., J. Plasma and Fusion Research **6**, (2004), 139.

[19] GARCIA, O.E., BIAN, N.H., FUNDAMENSTSKI, W., Phys. Plamas **13** (2006) 082309.

[20] D'IPPOLITO, D.A, MYRA, J.R, KRASHENINNIKOV, S.I., Phys. Plasmas **9** (2002) 222.

[21] RYUTOV, D.D., "The Dynamics of AnIsolated Plasma Filament at the Edge of a Toroidal Device", submitted to Phys. Plasmas.

[22] BERK, H.L., RYUTOV, D.D., TSIDULKO, YU. A., Phys. Fluids **B3** (1991) 1346, and BERK, H.L., COHEN, R.H., RYUTOV, D.D., TSIDULKO, YU. A., XU, X.Q., Nucl. Fusion bf 33 (1993) 263.

[23] COHEN, R.H., RYUTOV, D.D., Contr. Plasma Phys. **36** (1996) 161.